Journal of the Physical Society of Japan
Vol. 75, No. 10, October, 2006, 104602

Simulation of the Dependence of the Bulk-Stress–Strain Relations of Granular Materials on the Particle Shape

Salah A. M. El Shourbagy*,
Shinichi Morita and Hans-Georg Matuttis

Department of Mechanical Engineering and Intelligent Systems,
University of Electro-Communications, 1-5-1 Chofugaoka, Chofu, Tokyo 182-8585

(Received July 1, 2006; accepted August 10, 2006; published October 10, 2006)

We investigate the effect of particle shape and interparticle friction on the stress–strain-relation using the discrete element method (DEM) in two dimensions. Elongated particles show a significantly higher shear strength than non-elongated particles. The relative maximum which is characteristic for experimental stress–strain curves of granular materials is found only for elongated particles with finite Coulomb friction, which indicates that the particle elongation is an important parameter in the statistical physics of granular materials. An earlier simulation result from another group which showed a maximum for non-elongated particles could be identified to be due to the formation of a shear band.

KEYWORDS: granular media, non-spherical particles, discrete element method, stress–strain-relation, biaxial compression
DOI: 10.1143/JPSJ.75.104602

1. Introduction

Experimentally, stress–strain curves for granular material are determined via triaxial compression: The material is put in a rubber membrane, which in x, y-direction is held under constant pressure from an external water reservoir, while the volume is compressed in z-direction under constant velocity, see Fig. 1(a). The resulting characteristic stress strain curve [Fig. 2(a)] has a linear regime, followed by the non-linear plastic regime with the yield stress, the peak stress and the failure regime [Fig. 2(b)]. There, the stress necessary to deform the material is smaller than the peak stress, and the density-maximum (minimum of the volume) is not reached at the peak stress, but before, due to Reynolds dilatancy, see Fig. 2(b). Original, our interest in the problem was caused by the collaboration with an experimental group: We had asked for the measurement of stress–strain diagrams of monodisperse spherical and diamond-shaped plastic beads. The characteristic maximum in the raw data stress–strain diagram failed to develop, even for unreasonable large strains, which often lead to tearing of the membrane and created a mess in the laboratory.[1] The investigation was discontinued and we were asked to obtain further theoretical insight via computer simulations ahead of any further resumption of the experiments. In our simulations with the discrete element method (DEM) in two dimensions,[2] we replaced the rubber membrane by a wall held under constant pressure, see Fig. 1(b). We found that a relative maximum in the stress–strain curve appears only for elongated particles, but not for non-elongated and especially not for round particles.[2] We were unaware of simulations with comparable size dispersion by Volk *et al.*[3] where a relative maximum in the stress–strain curve indeed appeared in a similar setting with round particles, in contradiction of the experimental results cited above. In this article, we want to clear up this seeming contradiction, as in statistical physics, the properties of microscopic constituents should be reflected in the macroscopic behavior of their agglomerate in a unique fashion. The paper is organized as follows: In §2, we outline the simulation method, in §3 up to §3.5 we investigate the systematic dependence on the parameters, and in §3.6 we analyze the difference between our result and the one by Volk *et al.*[3]

2. Simulation

We are using a DEM-code[4] for two-dimensional polygons (inscribed into ellipses of various half axis lengths) with friction[5] where particles have three degrees of freedom, two for the linear motion and one for the rotation. When not mentioned otherwise, the coefficient for the Coulomb friction between particles and walls is the same as for the inter-particle friction to reduce the number of parameters. The Young modulus of the particles and the walls is 10^7 N/m where not mentioned otherwise; note that in two dimensions, both the Young modulus and the stress have the dimension of N/m. In the following sections, depending on convenience, the stress will be either be given in N/m or scaled by the external pressure σ_3 (for the "third", the z-direction, though we have no "second" direction). In our experience, this code gives results which are in good qualitative agreement with the experiment if the plane of the simulation is along a symmetry plane of the problem,[4,6,7] which should be the case for biaxial compression.[2] For the simulation of the biaxial compression, the system was compressed under constant velocity along the y-axis [Fig. 3(b)] with $v = 0.01$ m/s, while it was held under constant pressure along the x-axis at the left and right wall; the dependence on the numerical value of external pressure was studied systematically. We draw the strain ε_1 as the relative displacement of the lid $\varepsilon_1 = \delta l/l_{\rm init}$ from the initial system width $l_{\rm init}$. Because the system is discrete and inhomogeneous anyway, so that particles can move relative to each other in some parts of the system, while others are at relative rest, we abstain from more elaborate definitions, as there is not "differential" character of the strain. The stress σ_1 was measured on the ground plate, as is customary in the experiment.

The area of the particles varies by a factor of about 20, see

*E-mail: salah@miyazaki.mce.uec.ac.jp

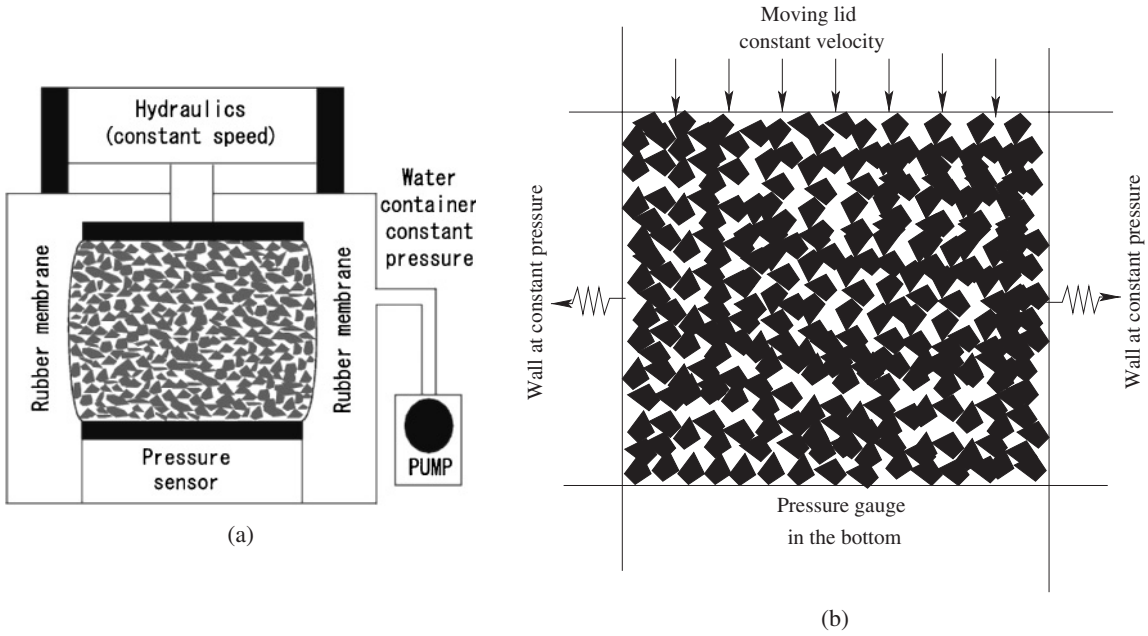

Fig. 1. Schematic drawing for triaxial and biaxial compression: (a) experimental and (b) computational.

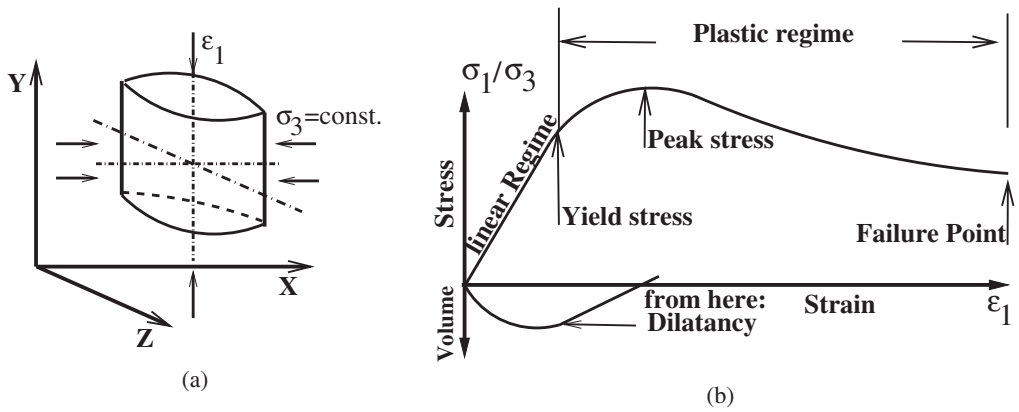

Fig. 2. Triaxial compression of granular materials: (a) strain (schematic) and (b) stress–strain-curve and density.

Fig. 4, so the average radius varies by a factor of about $\sqrt{20} \approx 4$. This distribution of diameters over less than one order of magnitude is termed "poorly graded" in the field of geotechnology. If the size distribution is extended to smaller particles in the sub-millimeter range, cohesion effects come into play. Though we have the necessary algorithms available,[8,9] we abstained from using smaller particles to limit our investigation to systems with purely repulsive interactions. Initially, the particles are dropped into the system from above, then the lid is lowered. Where not mentioned otherwise, the simulated system is initially approximately square [Fig. 3(a)], as in the experiment. While our simulation can be thought to go through the symmetry axis of the three-dimensional cylindrical test volume, Volk *et al.*[3] went a step further and fixed one wall as in Fig. 3(c), assuming that the left–right symmetry would not be affected by a boundary near the symmetry axis. Both kinematic situations[2,3] are different from that of García *et al.*,[10] where the system is purely stress-controlled. The simulations have been performed with about 1400 particles for systems with initial square cross section, while for the rectangular cross sections about 700 particles were used.

3. Compression and Stress–Strain Relations

Stress–strain diagrams are not "universal", but vary with the experimental conditions of the apparatus, e.g., the external pressure. As can be seen in Fig. 5(a), different curves are obtained both with a scaling in N/m [Fig. 5(a)] as well as by a rescaling with the external pressure [Fig. 5(b)] which is the reason why experiments on triaxial compressions are seldom published, but the measurements are used on a daily basis by geotechicians to determine the stability of soils. Because the influence of the walls is crucial as an external parameter, for these kind of systems finite size effects do not have to be considered.

3.1 Fluctuations and averaging noisy curves

As is typical for granular materials, the stress fluctuations in the raw data of the simulation are significant, see Fig. 6(a). These fluctuations are inherent in the system and

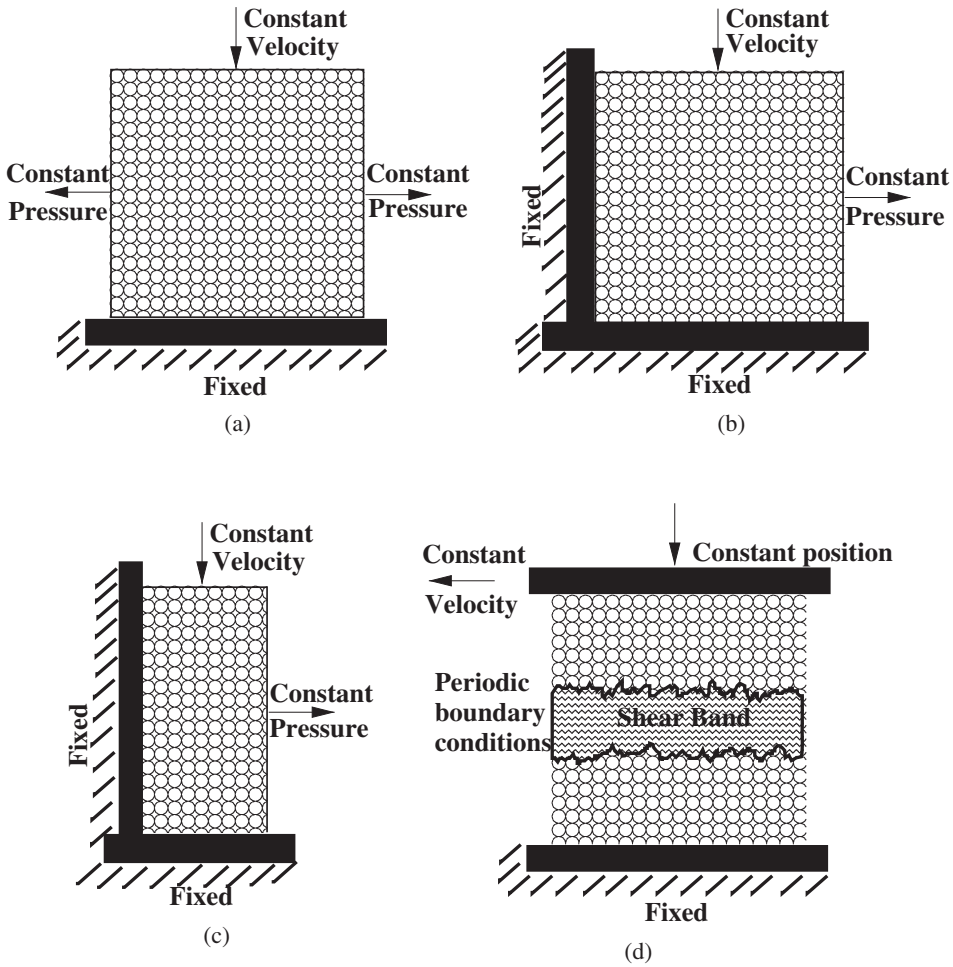

Fig. 3. Boundary conditions and geometries for the triaxial compression, as well as for the shear cell: (a) Our earlier work[2]. (b) Left boundary fixed. (c) Volk *et al.* (d) Simple shear.

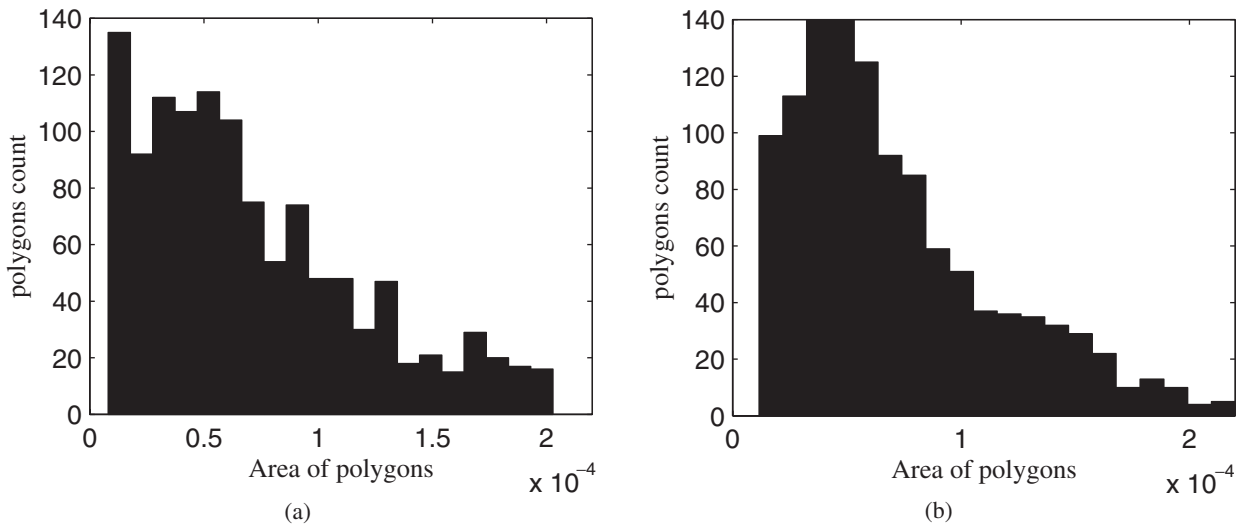

Fig. 4. Typical example of the size dispersion: Histogram of the area of poly-disperse heptagons (in m^2). (a) Elongation 1.0. (b) Elongation 1.8.

are also found in comparable experiments in three dimensions.[1)] Therefore, in the following, we give averages of several different runs (eight, where not mentioned otherwise) and their variance. Nevertheless, it may turn out for that some experiments the average of curves with a relative maximum is without maximum (because the maxima are at different positions). The opposite can also happen: A single sample with a significant maximum may cause the appearance of a maximum in an average while all other curves are flat. Therefore, in the following we will discuss both

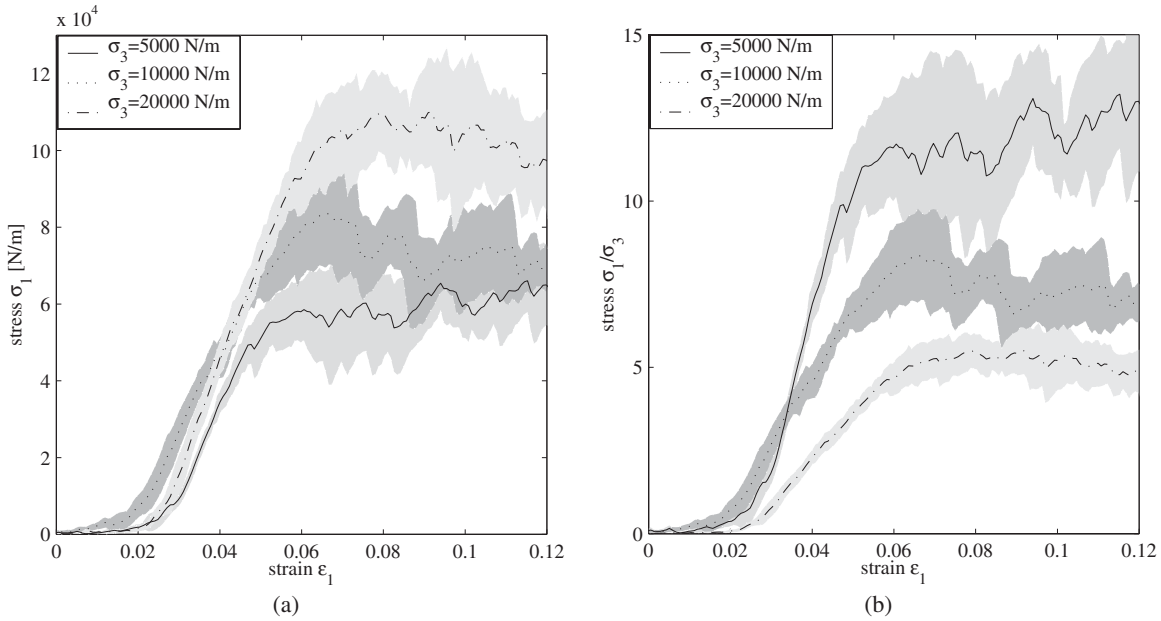

Fig. 5. Dependence of the average of stress–strain diagrams on the external pressure for non-elongated smooth particles (32 corners) and $\mu = 0.3$. The variance is indicated by shading. (a) Stress in N/m. (b) Stress scaled by σ_3.

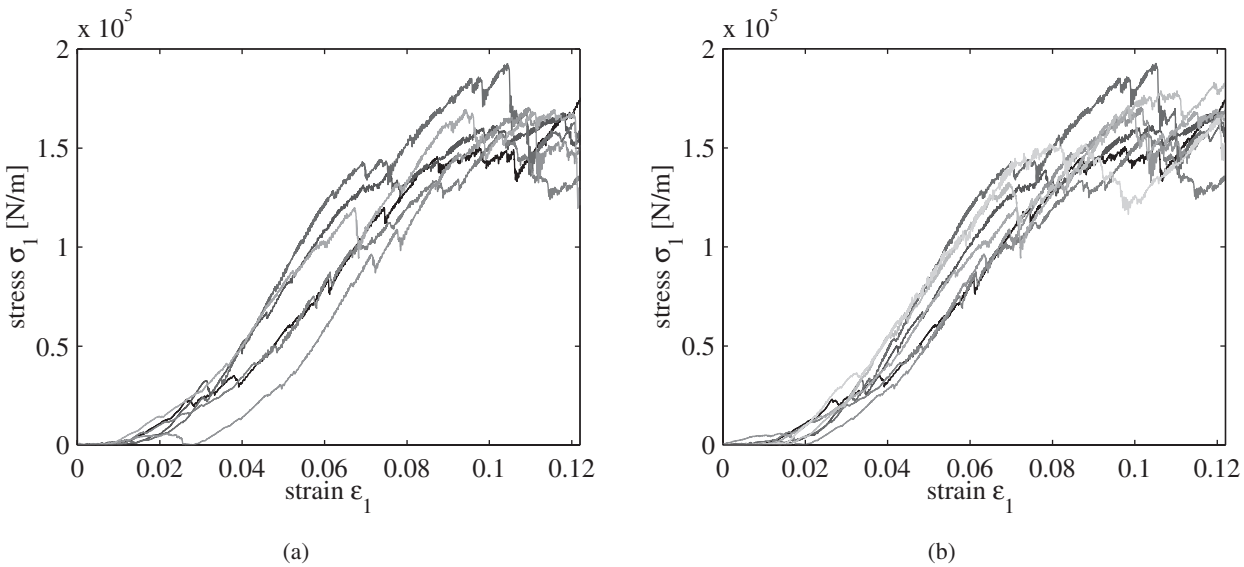

Fig. 6. Eight runs of stress–strain-curves for particles with elongation 1.8 with 15 corners, $\mu = 0.6$ and external pressure $\sigma_3 = 10000\,\mathrm{N/m}$. (a) $\varepsilon_1 = 0$ determined by the first contact between the lid and the particles. (b) The same data realigned along the slope.

averages, as well as curves for single runs. Another problem is that the starting configurations for the same parameters (friction, particle shape) may differ in their pore space. The point $\varepsilon_1 = 0$ might be welldefined as the position where the lid contacts the first particles, but the scattering of the data becomes significant [Fig. 6(a)], as the particle distribution in the system may be inhomogeneous. To reduce the resulting scattering, we aligned the curves along their slopes, see Fig. 6(b), so the data are independent of the initial particle distribution. In all following stress–strain diagrams, the variance of the 6 to 8 samples are shaded as in Fig. 5. This variance should be interpreted as a measure of the actual physical scattering of the data, not as an error bar which would vanish for an "infinite" amount of samples.

3.2 *Dependence on the particle elongation*

Figure 7(a) shows the stress–strain curves for particles with elongation 1.8 and 1.0. The maximal stress and the gradient in the linear regime increase with the particle elongation. This means that aggregates of non elongated particles have only half the stability of more of elongated particles. The characteristic feature of stress–strain-curves of granular materials, the maximum, is missing for non-elongated particles, which means that the failure-behavior of realistic granular materials like sand or gravel cannot be modeled by round or non-elongated particles. Though our simulations were performed only in two dimensions, the result seems to hold also in three dimensions, as in simulations of hard spheres and even van-der-Waals-poten-

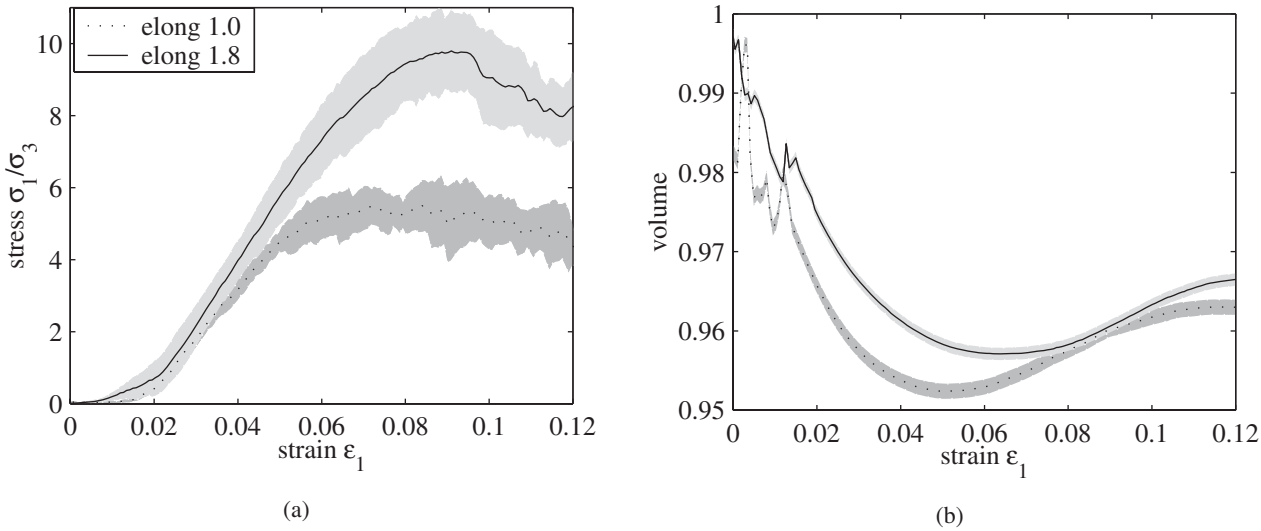

Fig. 7. Influence of the the particle elongation (32 corners, $\mu = 0.6$ and external pressure $\sigma_3 = 20000\,\mathrm{N/m}$). (a) Stress–strain diagram. (b) Volume–strain diagram.

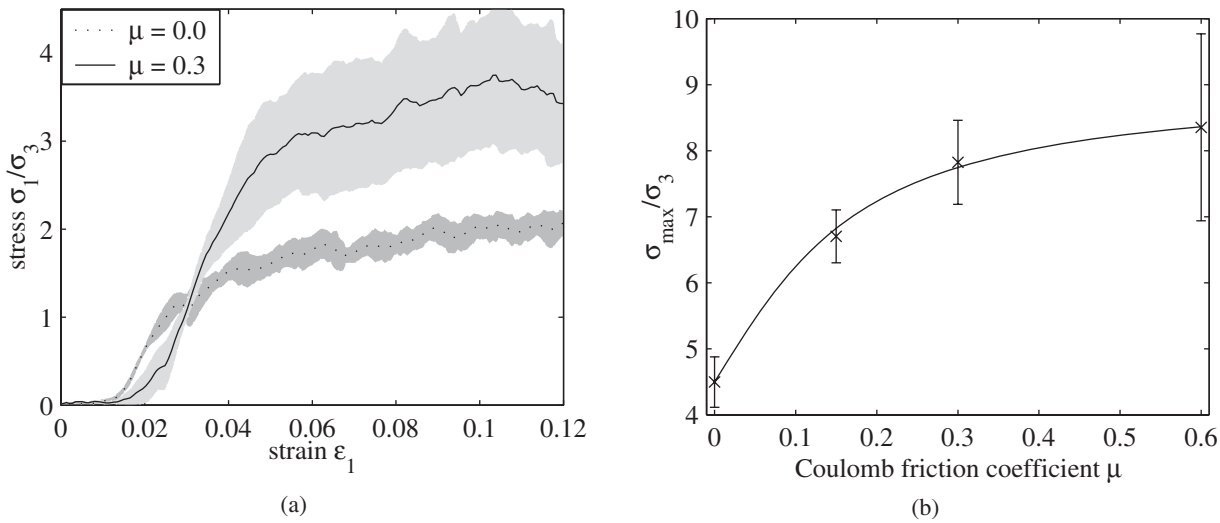

Fig. 8. Stress–strain behaviour for smooth polygons (32 corners) with average elongation 1.0 and external pressure $\sigma_3 = 10000\,\mathrm{N/m}$. (a) Averages for stress–strain curves with Coulomb friction coefficient $\mu = 0.0$ and 0.3. (b) Dependence of the maximum of the stress–strain curve on the Coulomb friction coefficient.

tials by Amin *et al.*[11] again no maximum of the stress–strain diagram was observed. Both for elongated and non-elongated particles, the density minimum (with the initial volume set to 1) occurs near the yield stress [Fig. 7(b)], independent of the occurance of a maximum in the stress–strain diagram. For strains up to $\varepsilon_1 = 2\%$, the reordering is still very marked, as can be seen from the density change in Fig. 7(b). When the regime of the yield-stress is approached, the volume–strain-curve is much less noisy than the corresponding stress–strain curve. The whole behavior of the material strength of granular materials from linear stress–strain over yield stress to failure happens in the rather narrow window of less than 5% density difference. As a note in the margin, for non-elongated, monodisperse particles no clear minimum in the volume–strain curve develops, but the volume decays monotonically up to $\varepsilon_1 = 0.5$ and then saturates.[2]

3.3 *Dependence on the friction coefficient*

Figure 8(a) illustrates the effect of the Coulomb friction coefficient μ on smooth particles with vanishing elongation. The maximal stress practically doubled for the increase from $\mu = 0.0$ to $\mu = 0.3$, though the size dispersion and the particle elongation were the same. For non-elongated particles and friction coefficient $\mu = 0.3$, the peak in the stress which should be characteristic for granular media (in contrast, e.g., to metals under uniaxial compression) is hardly visible [Fig. 8(a), full line]. For the same size- and shape-distribution at vanishing friction coefficient $\mu = 0.0$ [Fig. 8(a), dotted line], the stress–strain curves do not resemble those for granular materials: Not only is there no saturation of the maximal stress, but due to the curvature, the yield stress is practically unidentifiable. One has to conclude that for dense systems, simulations of particles with vanishing Coulomb friction do not really offer insights into

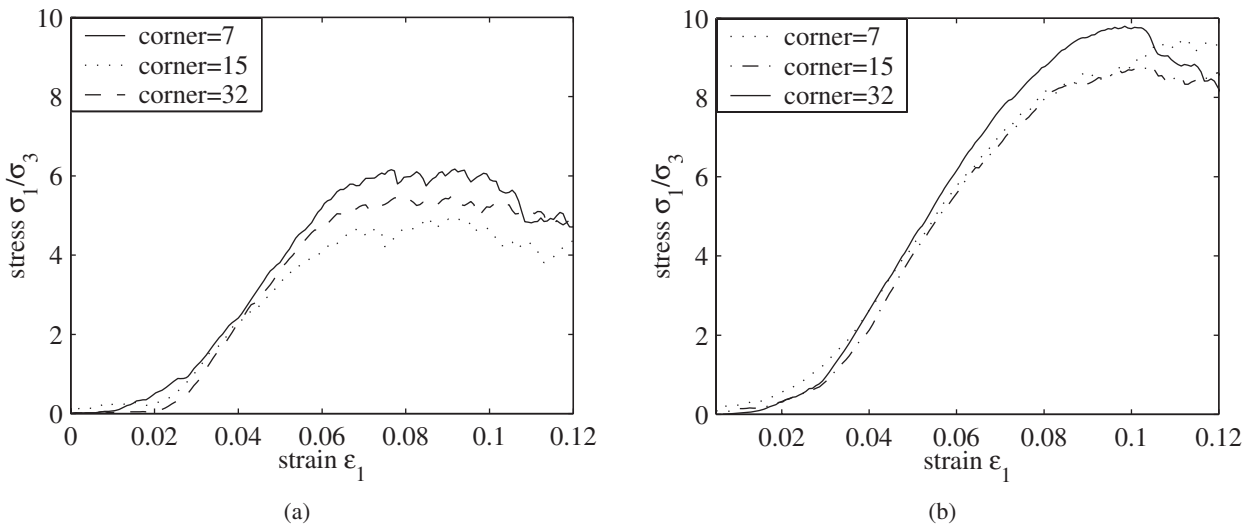

Fig. 9. Dependence of the stress–strain relations on the elongation, for different number of corners with about the same size dispersion, $\mu = 0.6$ and external pressure $\sigma_3 = 20000\,\mathrm{N/m}$. (a) Elongation 1.0. (b) Elongation 1.8.

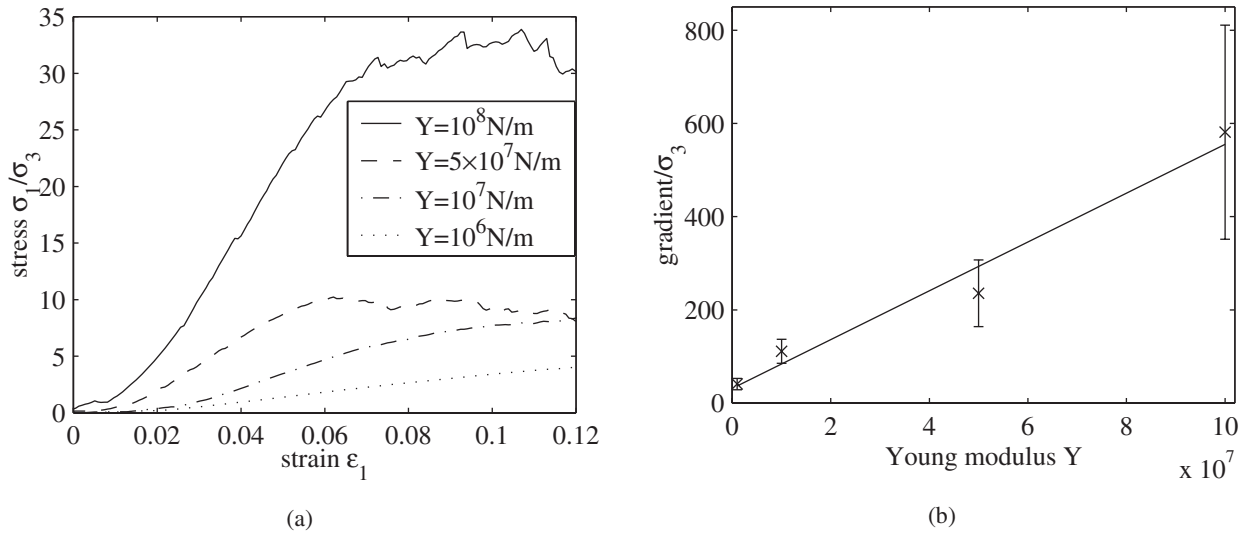

Fig. 10. Dependence of the peak stress on the Young modulus for poly-disperse polygons with elongated particles 1.8, $\mu = 0.6$ and 32 corners with external pressure $\sigma_3 = 40000\,\mathrm{N/m}$. (a) Stress–strain diagrams. (b) Linear fit.

the behavior of realistic granular materials. The μ-dependence of the maximum of the stress–strain-curve $\sigma_{\max}$ can be fitted to the functional form

$$\sigma_{\max}(\mu) = a \arctan(b\mu) + c \tag{1}$$

which yields the coefficients $a = 2.9 \times 10^4$, $b = 6.9$, and $c = 4.50 \times 10^4$ [Fig. 8(b)], which means that for about $\mu = 0.6$, $\sigma_{\max}$ saturates. This is the reason why we performed most of our simulation with $\mu = 0.6$.

3.4 *Dependence on the roughness of the particles*

Whereas the influence of the elongation on the stress–strain relation turned out to be considerable (§3.2), the effect of the number of corners was not so crucial. Figure 9 shows the stress–strain diagram for polygons with 7, 15, and 32 corners with different elongation, for the same average length and size-distribution as in Fig. 5(a). The fluctuations in the average of 6 to 8 samples are large enough so that the dependence of the curves is not monotonous. Though the "rough" non-elongated particles with 7 (full line) and 15 (dotted line) corners show something like a maximum in the strain-stress-relation, i.e., they are somehow realistic for granular materials, for smooth non-elongated particles the maximum is nearly non-existent. As the position of the maximal stress and and its numerical value for non-elongated particles are roughly independent of the number of corners, one can conclude that there is not much dependence on the macroscopic roughness. This is rather surprising, because intuitively, one associates a higher disposition to jam, i.e., shear resistivity with rougher surfaces. Though non-elongated polygons have a "rougher" appearance than spheres, and polygons with fewer corners look rougher than those with more corners, it should nevertheless be noted that our "roughness" is not on a microscopic scale, and the particles are still convex, and cannot latch onto each other. While for non-elongated

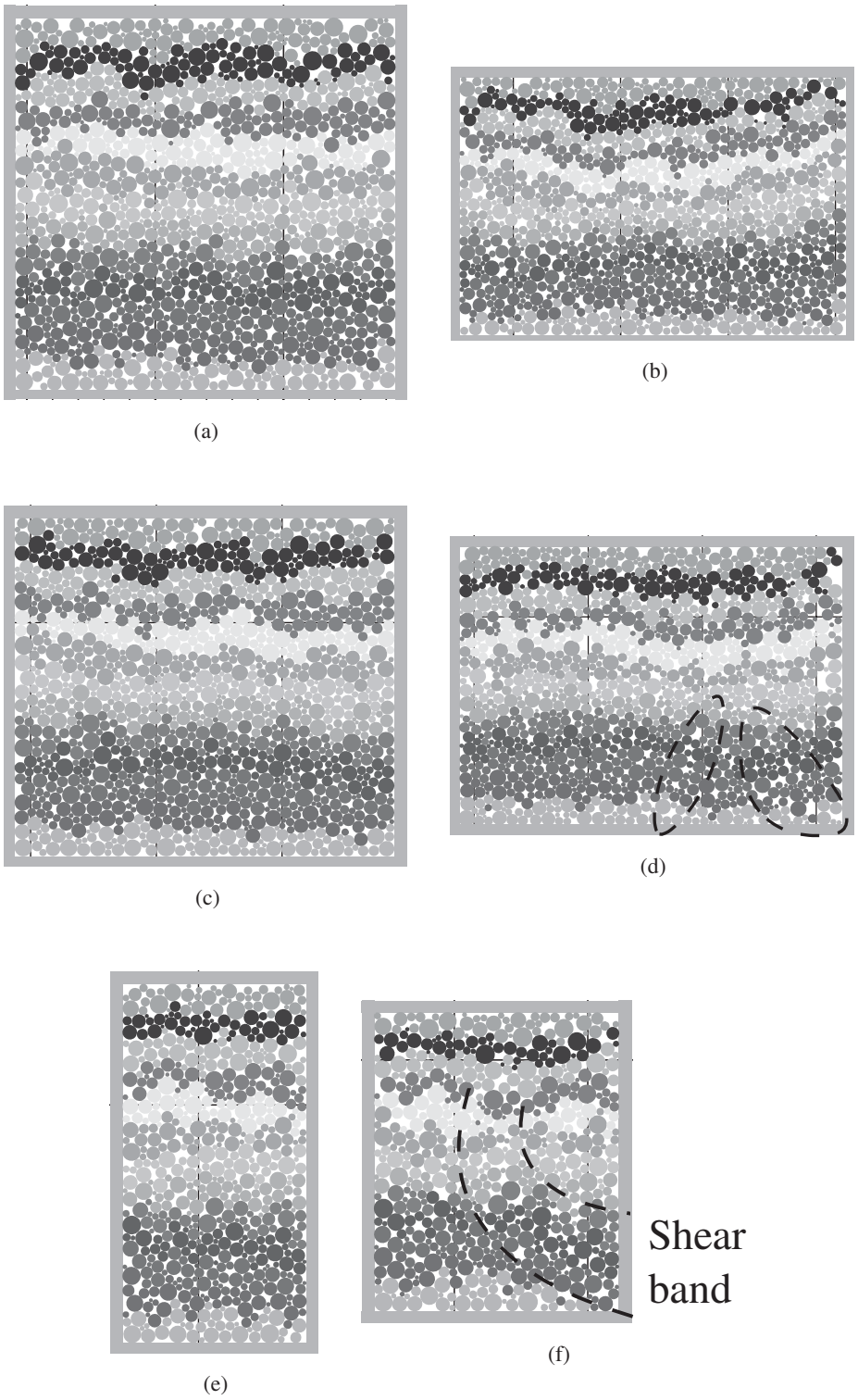

Fig. 11. Typical particle configurations for various boundaries conditions. Identical colors indicate equal layers during the filling process. (a) Both walls moving, initial configuration. (b) Both walls moving, final configuration. (c) Initial configuration with the left wall fixed. (d) Final configuration with the left wall fixed, some shear bands emphasized by dashed lines. (e) "Half" a system with the left wall fixed, initial configuration. (f) "Half" a system with the left wall fixed, final configuration.

particles, the pressure maximum was clearer for rough than for smooth particles [Fig. 9(a)], while in the case of elongated particles, the pressure maximum is clearer for smooth particles [Fig. 9(b)], where the fluctuations increase with the roughness, and the maximum is "smeared out". Ellipses show the same stress–strain behavior as smooth polygons of the same elongation.[2] Nevertheless, the gradient in the linear regime is independent from the number of corners, but depends on only the elongation.

3.5 *Dependence on the Young Modulus*

A somewhat disconcerting fact is that in contrast to other macroscopic quantities like, e.g., the angle of repose,[7] the stress–strain relation (both the maximal stress and the

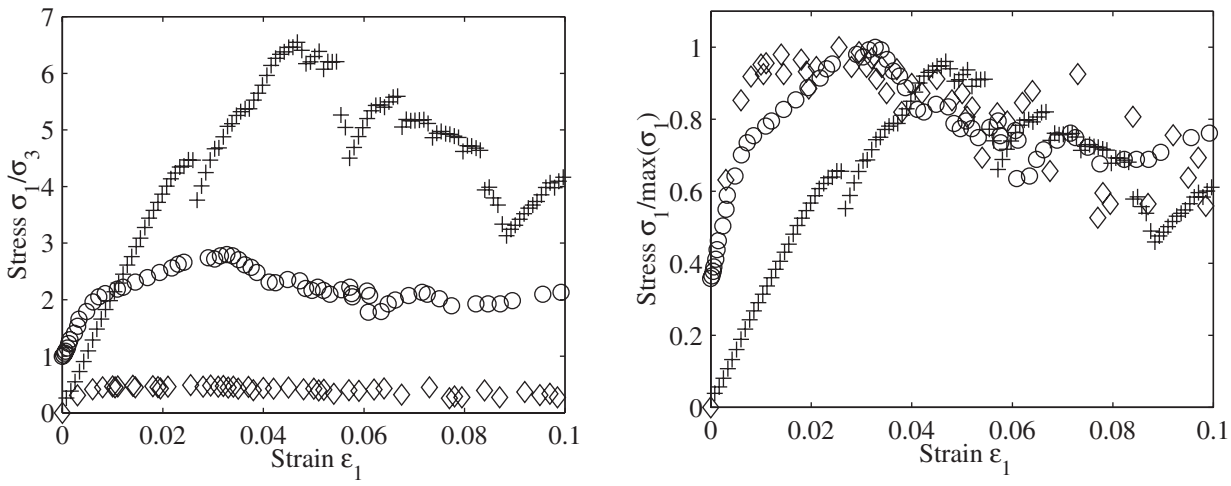

(a) (b)

Fig. 12. Results for the shearing simulation of Matsushima (diamonds), the biaxial compression of Volk *et al.* (circles) and our biaxial compression for a narrow system with fixed wall on one side (plus) for polydisperse polygons with elongation 1.0, 32 corners, $\mu = 0.6$, and $\sigma_3 = 40000\,\mathrm{N/m}$. (a) Scaled by the external pressure. (b) Scaled by the peak stress.

gradient of the linear regime) depends on the Young modulus of the material, see Fig. 10, even though the external pressure was at least two orders of magnitude lower than the Young modulus. The gradient in the linear regime increased linearly with the Young modulus within the fluctuations [Fig. 10(b)], and we found no saturation up to the highest Young modulus we used. This indicates that the mobilization of slip (sliding of one particle beyond the other) depends crucially on the hardness of the contacts.

3.6 Dependence on the boundaries

Finally, we want to investigate the effect of the boundaries, which was the initial question for this investigation. In the experiment for three-axial compression, the cross-section of the compression cell is usually square [Fig. 3(a)] and increases during the compression [Fig. 11(b)]. Because Volk *et al.*[3] (circles in Fig. 12) simulated only "half a system" where one wall was fixed due to symmetry consideration, their system was twice as high than it was wide, similar to our simulations in Fig. 11(e). For this system, Volk *et al.* (Fig. 12) got a clear maximum in the stress–strain relation for a single curve with non-elongated particles and a shear-band along the diagonal from upper left to lower right. Matsushima[12] got a similar maximum (diamonds in Fig. 12) for the simulation of a simple shear cell [see Fig. 3(d)]. For systems similar to those simulated by Volk *et al.*[3] with one wall fixed, we also get maxima for single curves [Fig. 13(f)] and the corresponding shear bands, as can be seen by the pattern in the layers [Fig. 11(f)]. In our simulation, the flow of the particles with one wall fixed [Figs. 11(d) and 11(f)] does not show the same layering structure as that with two moving walls [Fig. 11(b)]: The layer boundaries are tilted, because the fixed wall inhibits the flow of particles, both for "wide" [Fig. 11(d)] and "narrow" systems [Fig. 11(f)]. We also performed reference simulations where the friction coefficient of the fixed wall was set to 0: Within the fluctuations, the stress–strain diagram and the configurations were practically unchanged in comparison with finite friction. This means that the impenetrability constraint set by the wall has a stronger effect than its friction. We conclude that the maximum in the stress–strain relation in Volk *et al.*[3] is not due to granular material properties, but due to a shear band induced by the boundary conditions. For systems of twice the width and one wall fixed [Figs. 3(b) and 11(c)], the maximum in the stress strain relation for the single curve becomes unidentifiable [Fig. 13(c)] though shear bands can still be found [Fig. 11(d)]. For a system [Fig. 11(b)] with both walls moving, which are the "truly" physical boundary conditions, we get no maximum in the stress–strain relation, neither "on average" [Fig. 13(a)], nor in the single runs [Fig. 13(d)].

4. Conclusions

Agglomerates of non-elongated particles have only about half the strength of those with elongated particles. Simulations of non-elongated or round particles are therefore unsuitable to predict the experimental behaviour of realistic granular materials. For vanishing Coulomb friction between particles, the obtainable stress–strain curves do not resemble those of granular materials at all.

For finite Coulomb friction, the comparison with the simulation by Matsushima[12] suggests that the maximum in the simulation by Volk *et al.*[3] for non-elongated particles is due to a shearband, which is induced by fixing the left wall: The resulting peak stress is not characteristic for the material itself, only for the chosen boundary condition. The flow of the grains when one wall is fixed differs significantly from the situation where two walls are moving, so it is not possible to obtain the physical behavior of a "full" system by inserting a wall at the "symmetry axis" and simulate the remaining "half system". For realistic boundary conditions, single stress–strain curves show clear maxima for the peak stress only for elongated particles, even if those are only "pooly graded". For non-elongated particles, maxima in the stress–strain curves appear only "on average" for "extremely large" external pressures. This means that for the statistical physics of granular materials, the elongation is

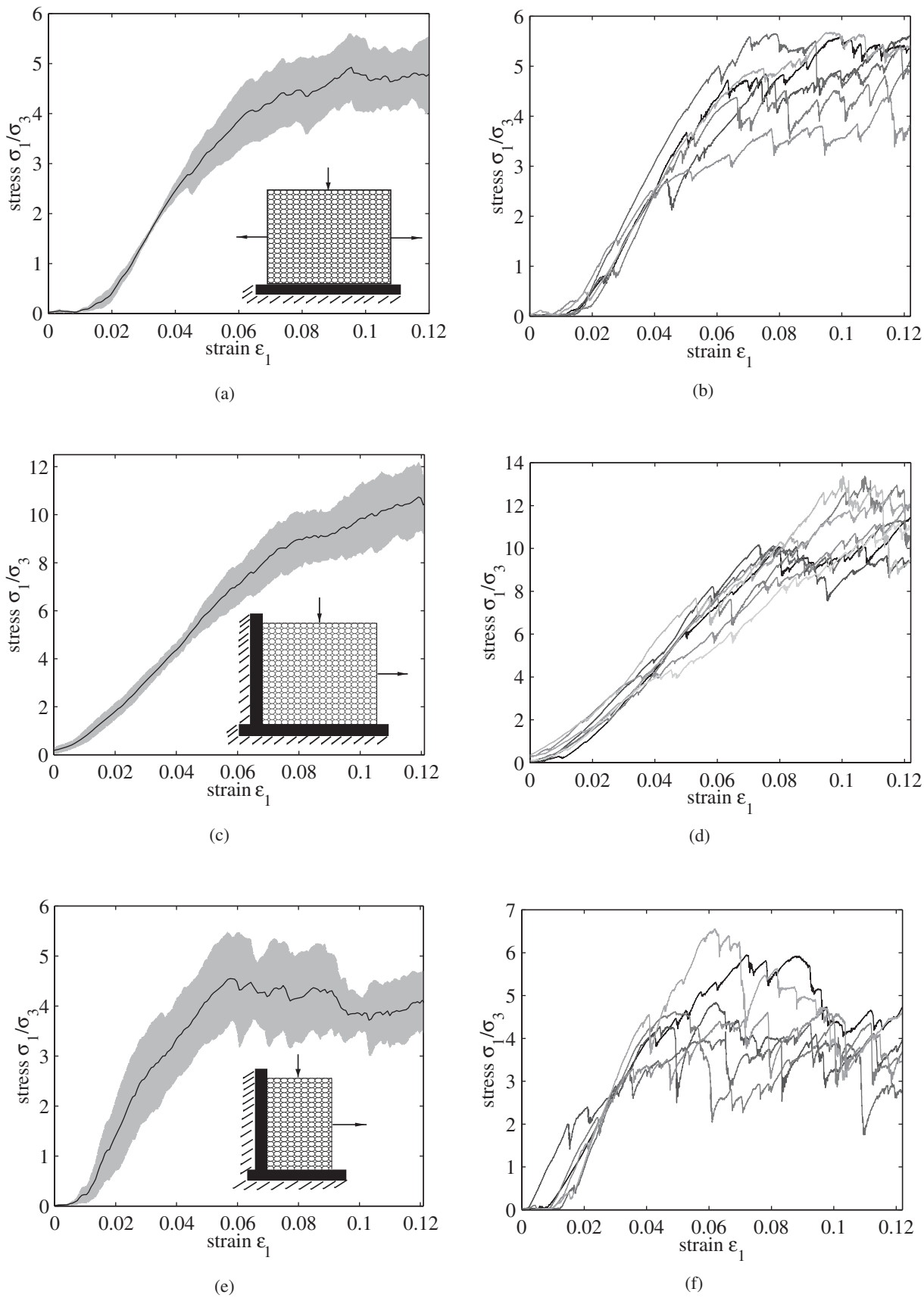

Fig. 13. Stress–strain relation of polydisperse polygons with elongation 1.0, 32 corners, $\mu = 0.6$, and external pressure $\sigma_3 = 40000\,\mathrm{N/m}$ for the boundary conditions given in the inset. (a) Both walls moving, average. (b) Ibidem, raw data. (c) One wall fixed, average. (d) Ibidem, raw data. (e) Half a system, one wall fixed, average. (f) Ibidem, raw data.

indeed a relevant microscopic particle parameter which effects the properties of the macroscopic bulk crucially. While the angle of repose depends not only on the particle elongation, but also on the roughness of the particles,[7] the averages of the stress–strain diagram are hardly affected by the particle roughness.

Acknowledgment

S.E.S. received a Student Services Organization (JASSO) scholarship during the writing of this paper.

1) S. Diebels: personal communication (1999).
2) H.-G. Matuttis, N. Ito and A. Schinner: *Proc. RIMS Symp. Mathematical Aspects of Complex Fluids III* (RIMS, Kyoto Univ., Kyoto, 2003) RIMS Kôkyûroku, No. 1305, p. 89.
3) W. Volk, S. Diebels, M. Lätzel and S. Luding: Rep. Inst. Mech. (Bauwesen), University of Stuttgart, No. II-7, p. 121(2001) [in German].
4) H.-G. Matuttis: Granular Matter **1** (1998) 83.
5) P. A. Cundall and O. D. L. Strack: Geotechnique **29** (1979) 47.
6) H.-G. Matuttis, N. Ito, H. Watanabe: *Proc. Traffic and Granular Flow* (Springer, Berlin, 2003) p. 455.
7) S. A. M. El Shourbagy and H.-G. Matuttis: *Proc. Powders and Grains* (Balkema, Leiden, 2005) Vol. 2, p. 1289.
8) H.-G. Matuttis and A. Schinner: Int. J. Mod. Phys. C **12** (2001) 1011.
9) A. Schinner and H.-G. Matuttis: *Proc. Traffic and Granular Flow* (Springer, Berlin, 1999) p. 505.
10) R. García-Rojo, S. McNamara, A. A. Peña and H. J. Herrmann: *Proc. Powders and Grains* (Balkema, Leiden, 2005) Vol. 1, p. 705.
11) M. Amin and S. J. Antony: Comput. Mater. Sci. **36** (2006) 381.
12) T. Matsushima: Proc. JSCE/EqTAP Workshop Seismic Fault-induced Failures, 2003, p. 97.